AAS 13-787

BROAD SEARCH FOR UNSTABLE RESONANT ORBITS IN THE PLANAR CIRCULAR RESTRICTED THREE-BODY PROBLEM

Rodney L. Anderson,* Stefano Campagnola,† and Gregory Lantoine*

Unstable resonant orbits in the circular restricted three-body problem have increasingly been used for trajectory design using optimization and invariant manifold techniques. In this study, several methods for computing these unstable resonant orbits are explored including flyby maps, continuation from two-body models, and grid searches. Families of orbits are computed focusing on the Jupiter-Europa system, and their characteristics are explored. Different parameters such as period and stability are examined for each set of resonant orbits, and the continuation of several specific orbits is explored in more detail.

INTRODUCTION

The computation of unstable resonant orbits in the circular restricted three-body problem (CRTBP) has increasingly been used as a basic component of trajectory design using both invariant manifolds and optimization techniques. In particular, these types of orbits have become more of a focus for tour design in multi-body environments as three-body effects have been incorporated earlier in the mission design process. In the past, tour design within these environments has relied heavily on two-body or patched-conic methods,[1–3] and some effects of the three-body problem have been included using a variety of techniques[4,5] including optimization tools.[6,7]

Early work that indicated that unstable resonant orbits could be useful in this process was done by Schroer and Ott.[8] They built on Bollt and Meiss's[9] study by targeting the invariant manifolds of resonant orbits to reduce transfer time for Earth-Moon transfers. Anderson and Lo then showed that the invariant manifolds of unstable resonant orbits were important in ballistic,[10] impulsive,[11] and low-thrust trajectories.[12] Resonant orbits themselves have been used directly as initial guesses in combination with optimization algorithms to successfully design tours by Lantoine, Russell, and Campagnola.[13] The invariant manifolds of these types of resonant orbits have also been used to design trajectories that traverse multiple resonances for the endgame problem,[14] across multiple CRTBPs,[15] and for approach.[16,17] Resonant orbits have been examined in the Earth-Moon system[18] and used for various transfers[19] including transfers to libration point orbits.[20] Barrabés and Gómez examined second species solutions obtained from $p - q$ resonant orbits for the planar and spatial cases.[21–23] Three-dimensional resonant orbits have also been explored by Vaquero and Howell.[24] Studies of other types of periodic orbits in the CRTBP have been undertaken in the past by Henon,[25,26] Broucke,[27,28] Strömgren,[29] Szebehely,[30] and Russell[31] among others.

The variety of successful applications of these techniques to trajectory design indicates that obtaining a deeper understanding of resonant orbits will be a fruitful avenue to pursue in further developing these methods. The fact that these techniques have been so successful also suggests that the dynamical channels computed as a result of understanding these resonant orbits may provide a more fundamental understanding of transport within the solar system with broader applications within celestial mechanics. As previously stated, specific sets of unstable resonant orbits have been presented in the past with the focus on the types of orbits relevant to specific applications. In this study, an exploration of new resonant orbits and techniques for computing them are presented with an emphasis on describing resonant orbit characteristics for different

*Member of Technical Staff, Jet Propulsion Laboratory, California Institute of Technology, 4800 Oak Grove Drive, M/S 301-121, Pasadena, CA 91109

†International Top Young Fellow, Institute of Space and Astronautical Science, Japan Aerospace Exploration Agency

systems and energies. Various techniques for computing unstable resonant orbits are first discussed, and orbits with close approaches to the secondary in the system are emphasized. These include continuation from cases with small mass parameters, grid searches, and a flyby map technique. Both the flyby map technique and the grid search can be used to visually search the space for new trajectories that may be useful. Specific families are examined in more detail and characteristics of these families are discussed. The continuation of several families of orbits are then analyzed in more detail.

BACKGROUND

Circular Restricted Three-Body Problem

All of the periodic orbits presented in this paper are computed in the circular restricted three-body problem (CRTBP).[30] In this model the motion of an infinitesimal mass is computed in a system with two massive bodies orbiting one another in circular orbits. The equations of motion of the infinitesimal mass may be written in a rotating frame as

$$\begin{aligned} \ddot{x} - 2\dot{y} &= \frac{\partial \Omega}{\partial x} \\ \ddot{y} + 2\dot{x} &= \frac{\partial \Omega}{\partial y} \\ \ddot{z} &= \frac{\partial \Omega}{\partial z} \end{aligned} \tag{1}$$

where

$$\Omega = \frac{x^2 + y^2}{2} + \frac{(1-\mu)}{r_1} + \frac{\mu}{r_2} \tag{2}$$

and

$$r_1 = \sqrt{(x+\mu)^2 + y^2 + z^2},\ r_2 = \sqrt{(x-1+\mu)^2 + y^2 + z^2}. \tag{3}$$

The rotating frame is aligned with the massive bodies with the x axis pointing from the larger body (the primary) to the smaller body (the secondary). The y axis then points in the direction of motion of the secondary, and the z axis completes the right-handed coordinate frame. The mass of the primary is $1-\mu$, and the mass of the secondary is μ. The coordinate frame is centered on the barycenter so that the primary is located at $x = -\mu$, and the secondary is located at $x = 1-\mu$. In this paper the majority of orbits are computed in the Jupiter-Europa system with some interior resonant orbits given in the Jupiter-Ganymede system. The values used here for these systems are given in Table 1.

Table 1. Mass ratios for the Jupiter-Europa and Jupiter-Ganymede CRTBP systems

System	μ
Jupiter-Europa	0.0000252664488504
Jupiter-Ganymede	0.0000780369094055

Five equilibrium points are found in the problem with three collinear points located along $y = 0$ and two triangular equilibrium points located an equal distance from the primary and the secondary. The constant of motion for the CRTBP is referred to as the Jacobi constant and is computed using

$$\mathrm{C} = 2\Omega - \mathrm{V}^2 = x^2 + y^2 + \frac{2(1-\mu)}{r_1} + \frac{2\mu}{r_2} - \dot{x}^2 - \dot{y}^2 - \dot{z}^2. \tag{4}$$

Single-Shooting Method and Continuation

Periodic orbits in the CRTBP may be computed using one of the symmetry properties of the CRTBP.[32,33] Using this property, if an orbit in the planar CRTBP (PCRTBP) intersects the $y = 0$ line perpendicular to this line in two different points, the orbit will be a symmetric, periodic orbit. This property provides the basis for

a single-shooting algorithm[34,35] that uses the variational equations to update an initial guess for a periodic orbit until a truly periodic orbit is obtained. The algorithm used to compute the orbits in this study is an adaptation of this single-shooting technique.

Several different continuation methods are used for this study. The simplest method is to take a solution obtained using the single-shooting method and increment the initial solution using small steps in x. After incrementing, the previous solution is used as the initial guess for the new solution, and the new orbit is computed with this initial guess. If the orbit is not very unstable and the step size used for x is small, this technique often works well. If larger step sizes are desired, then an extrapolation using data from previous solutions may be used. For situations where fold points occur in the continuation, the pseudo-arclength[36] continuation methods implemented in AUTO[37] are used.

Unstable Resonant Orbits

This study is primarily concerned with unstable resonant orbits although the techniques discussed here may be used to compute stable resonant orbits, and some stable resonant orbits are presented during the analysis. We are specifically interested in unstable resonant orbits because they possess invariant manifolds that theoretically provide free transfers between different unstable orbits in the CRTBP, and they have been found to be useful for initial guesses in optimization algorithms. The type of resonance that is the focus of this paper may be described as mean motion resonance which may be most easily understood in a two-body context. In the two-body problem, this type of resonance occurs when the periods of two orbits can be related by an integer ratio. If a point mass is placed on an elliptical orbit in the three-body rotating frame so that it travels around the primary p times in the inertial frame for every q times the secondary completes a revolution around the primary where $p, q \in \mathbb{N}$, then the elliptical orbit will be periodic in the rotating frame. The resonant integers, the mean motions, and the periods of the point mass and the secondary may be related by

$$\frac{p}{q} = \frac{n_p}{n_q} = \frac{\mathbb{P}_q}{\mathbb{P}_p}. \tag{5}$$

The form p:q is used to designate resonances in this paper, which is the same as *point mass revolutions* : *secondary revolutions*. Exterior resonances correspond to trajectories that have a period greater than that of the secondary while interior resonances are defined as those that have a period less than the secondary. *Loops* develop at the apses of some of these trajectories in the rotating frame for particular eccentricities and aid in determining the potential resonance of the trajectory. Samples of the type of behavior that might be observed for resonant orbits in the rotating frame computed in the two-body problem are given in Figure 1. The

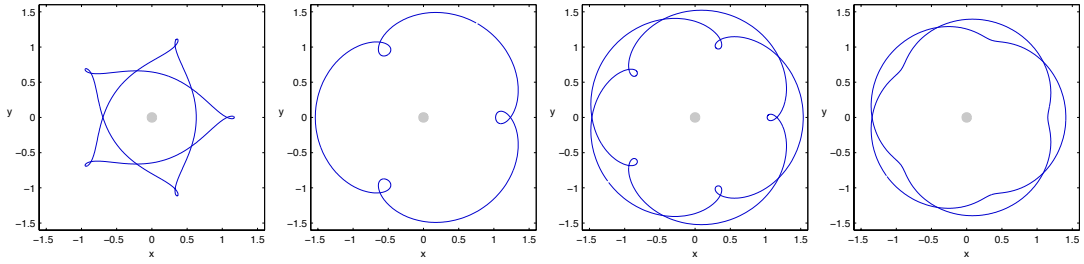

(a) 5:3, e = 0.3 (b) 3:4, e = 0.2 (c) 5:7, e = 0.2 (d) 5:7, e = 0.1

Figure 1. Selection of two-body resonant orbits plotted in the rotating frame to illustrate their characteristics. Note that the orbit in (b) is a first order resonance, while the other orbits are second order resonances.

expected loops can be observed for each resonant orbit, and the number of loops corresponds to the number of periapse or apoapse passages of the infinitesimal mass. The interior resonant orbit loops in Figure 1(a) occur at apoapse, and the exterior resonant orbit loops occur at periapse. Notice that for some eccentricities the loops do not occur. See Murray and Dermott for a fuller explanation of these characteristics.[38]

Most of these characteristics apply to both two-body and three-body resonant orbits, but in the case of the three-body problem, the periods are no longer related by a strict integer relationship. In this case the relationship becomes approximate as given by Murray and Dermott:[38]

$$pn_p \approx qn_q. \tag{6}$$

Given this approximate relationship, it is sometimes helpful to observe the orbit intersections in a Poincaré section.[11,39] This technique is especially helpful for stable orbits, which can be observed at the center of islands representing quasi-periodic orbits in the chaotic sea. Unstable resonant orbits intersect within this chaotic sea, but once the intersections have been computed, they may be compared to the stable resonances. In the CRTBP, the infinitesimal mass on a resonant orbit will in general not return to the same point after q revolutions of the secondary, and this effect will typically be larger for those trajectories that loiter near the secondary. The difference in period can lead to some difficulties in finding the resonance for the orbit.

Determining the resonance of an orbit in the CRTBP is sometimes more challenging than it appears at first. The difficulty arises from the fact that the period varies from an exact integer ratio in the CRTBP. For those orbits that may be continued from existing orbits in the two-body problem, the resonance may be defined based on the exact resonance of that orbit in the two-body problem. If the osculating period of such an orbit is found at a location where the point mass is far from the secondary, the period is often near the integer ratio of the selected resonance. Note that the period found here has typically been used to designate the resonance of an orbit for mission design purposes. The period is not necessarily always near the expected integer ratio, however, and as the orbit is continued across the mass parameter and across Jacobi constant the period can vary noticeably. When the osculating period of the orbit is computed with respect to the barycenter, the period will also jump significantly if any close approaches to the secondary occur. For those orbits that are computed via numerical search, the designation of the resonance becomes more difficult. Typically, the assignment of a resonance is based on a combination of the osculating period computed far from the secondary evaluated across the family and the number of periapses that have occurred for the point mass. Selecting the resonance becomes less precise however when unusual orbits are found that may make multiple passes near the secondary. In general, it is useful to keep both the osculating, distant, two-body period and the actual period of the selected orbit in mind.

Another question in the analysis of resonant orbits that naturally arises is how should they be classified? Some classification schemes already exist, although many that exist for the CRTBP are tailored more for libration point orbits or simpler orbits than those that are being studied here. Broucke[27] introduces one classification scheme based on the location of the perpendicular intersections of a periodic orbit. Using this classification, interior resonant orbits would be class 2 orbits, and exterior resonant orbits would be class 3 orbits.

One further question when exploring resonant orbits is which resonant orbits are of the most interest? In the Jupiter-Europa system it was known from early work with patched-conic methods that the 3:4-5:6 resonant sequence was important for approaches to Europa,[40] and specific unstable resonant orbits were shown to be important in this process.[11] Other resonant orbits have also been computed for different systems including Jupiter and various Jovian moons,[10–13,41–43] the Earth-Moon system,[18–20] and Saturn-Titan.[19,24,43] Comets have also been known to follow resonances,[44,45] and the general idea of using resonance was also found in standard techniques based on two-body or patched-conic methods.[46] The dominant type of resonant orbit computed for these is derived from an equivalent two-body orbit, and often has a loop near the secondary. Specific resonant orbits have been noticed however that possess multiple loops near the secondary. These types of orbits have particular characteristics that make them more suitable for approach trajectories, and the multiple loops may make them ideal for spacecraft attempting to observe the secondary. As mentioned previously, one focus of this paper is to examine these types of orbits.

CONTINUATION FROM TWO-BODY ORBITS

One of the more straightforward ways to compute unstable resonant orbits is to continue known solutions from the two-body problem into the CRTBP. These types of solutions are discussed in general by Hénon,

and the generating orbits used to compute these types of orbits are classified as first species, second kind.[25] It is straightforward to compute an initial state for an orbit with the desired resonance using the two-body equations of motion by first computing the semimajor axis as

$$a = \left(\frac{\mathbb{P}}{2\pi}\right)^{2/3} = \mathbb{P}_n^{2/3} \tag{7}$$

where $\mathbb{P}_n$ is the normalized period of the desired orbit ($\mathbb{P}_n/\mathbb{P}_{secondary} = \mathbb{P}_n/2\pi$). Then the dimensionless velocity magnitude at periapse or apoapse on the $y = 0$ line may be computed as

$$|v| = \sqrt{2\left(\frac{-1}{2a} + \frac{1}{x}\right)}. \tag{8}$$

With this initial guess, the orbits may be continued using mass to obtain the orbit in the desired system. This method is generally robust, but it only produces a particular set of orbits that are derived from those obtained in the two-body problem. Sometimes this initial guess may be used as an initial guess for an orbit in the CRTBP with the mass ratio of interest, but often convergence issues arise, and the resulting orbit is not at the desired resonance.

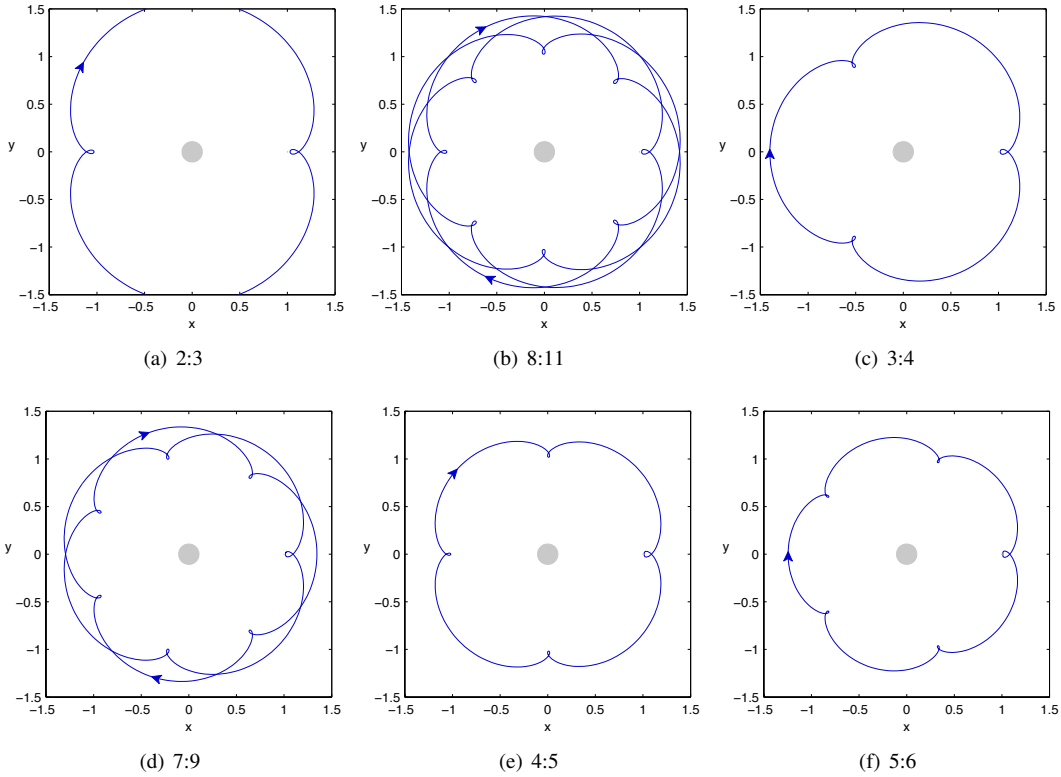

(a) 2:3 (b) 8:11 (c) 3:4

(d) 7:9 (e) 4:5 (f) 5:6

Figure 2. Selection of exterior resonant orbits in the Jupiter-Europa system (rotating frame) at C = 3.0 obtained from generating orbits classified as first species, second kind.

The majority of orbits used as resonant orbits for tour design in the literature appear to fall in this category, and several computed examples are given in Figure 2 for external resonances in the Jupiter-Europa system. A sample of some interior resonances computed for the Jupiter-Ganymede system are given in Figure 3. It can be seen from these plots that these orbits in general possess similar characteristics. For these cases, they all have a single loop or close approach to the secondary once each period.

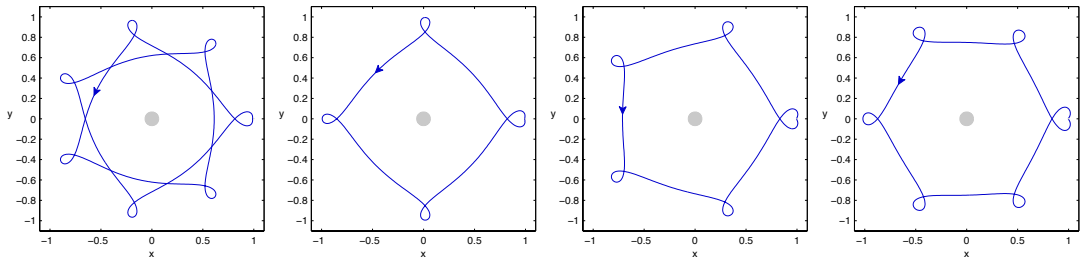

(a) 7:5 (b) 4:3 (c) 5:4 (d) 6:5

Figure 3. Selection of interior resonant orbits in the Jupiter-Ganymede system (rotating frame) at C = 2.99 obtained from generating orbits classified as first species, second kind.

GRID SEARCH USING A SINGLE-SHOOTING METHOD

While the majority of resonant orbits that have been used so far for trajectory design are continued from two-body orbits, a more complex type of orbits obtained using numerical searches have been found to be useful for particular applications.[41] In particular, one orbit near the 5:6 resonance found using a grid search was found to be particularly relevant to understanding the planar Europa orbiter's approach to Europa in Anderson and Lo.[11,41,47] A portion of the family corresponding to those types of orbits is shown in Figure 4(a) for the Jupiter-Europa system, and a similar family is shown in Figure 4(b) for the Jupiter-Ganymede system at a different resonance. It can be seen from the flyby characteristics that these types of orbits may have potential applications for mission design and observations of the secondary. It has also been shown that the invariant manifolds of this orbit could be used to compute a direct approach to Europa.[16] It is the search for these types of resonant orbits that has motivated the majority of the current work.

A grid search method built around a single-shooting algorithm is discussed here in general and a sample of the results are presented. A fine search using these methods results in a large number of orbits that can be culled using various criteria to reduce the database. The resulting orbits may then be examined visually to search for orbits that may be of interest for a particular application. The first criteria generally used here is that the search is limited to unstable orbits, and because flyby orbits are of the most interest, the focus is on trajectories that make close approaches to the secondary.

A grid search may be performed using several different approaches. The results in each case will vary based on the interaction of the initial guess and the differential corrections algorithm, and the resulting solutions may appear in different areas depending on the method. One option is to start with a fixed value for x with $\dot{x} = y = 0$. Various values of $\dot{y}$ may then be used as initial guesses for a periodic orbit. The initial guess is used with a single-shooting method to converge on a periodic orbit that is symmetric with respect to the $y = 0$ line. x may then be incremented and the process repeated. In each case, the intersection number with the $y = 0$ line at which a perpendicular crossing is searched for needs to be specified as an input for the single-shooting algorithm. The converged solutions for each initial guess of x and $\dot{y}$ may then be evaluated to determine their characteristics. In this search we are primarily interested in unstable orbits with lower time-of-flights (TOFs), and the orbits are evaluated using these criteria along with a visual inspection.

In his study, Broucke gives an estimate of the range of $\dot{y}$ values that should be searched based on the desire for the two-body energy to be less than zero as

$$-x_0 - \sqrt{2(\frac{1-\mu}{r_1} + \frac{\mu}{r_2})} \leq \dot{y}_0 \leq -x_0 + \sqrt{2(\frac{1-\mu}{r_1} + \frac{\mu}{r_2})} \tag{9}$$

For this study though, our focus is on unstable orbits with close approaches to the secondary, so while this range was a useful guide, it was often found that a small portion of the range was of the most interest. For these analyses, an initial broad range with a rough grid was often initially searched, and then a finer grid over areas that appeared to give periodic orbits was used to examine particular areas of orbits in more detail.

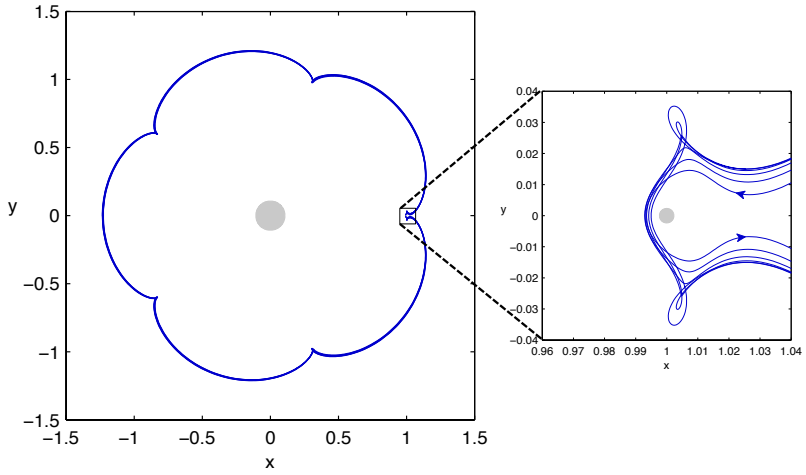

(a) Jupiter-Europa 5:6 Resonant Orbit Family

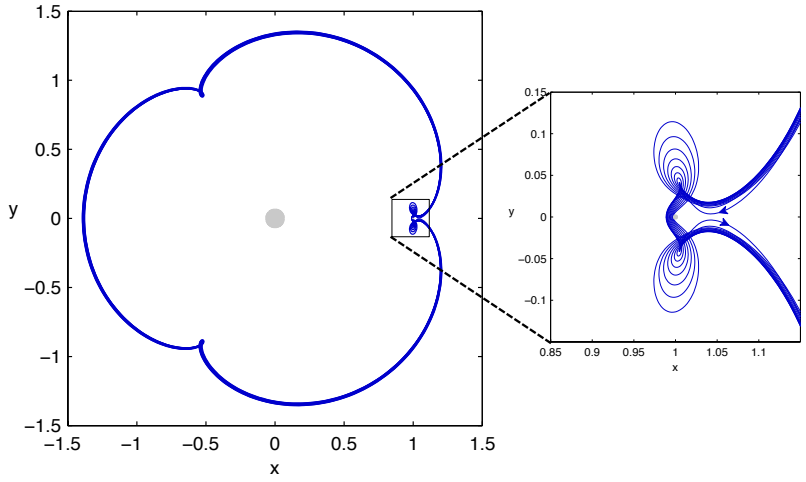

(b) Jupiter-Ganymede 3:4 Resonant Orbit Family

Figure 4. Example of orbit families in different systems at different resonances with similar characteristics of loops in the orbit near the secondary.

To obtain a better understanding of the search process, it is useful to examine the details of the solutions evaluated for a particular x. The results presented here are limited to those with the number of intersections equal to four (not including the initial point). The same technique has been successfully applied to trajectories with other intersections, but it is not feasible to present all of those results here. The details discussed here for these cases are representative of the results that are obtained for other cases. Although it might be expected that similar values of $\dot{y}$ used as an initial guess would result in similar solutions, this is not necessarily the case. The actual converged orbit depends on the combination of this initial guess and the correction algorithm that is used. Results for a case with $x = 1.01$ using the specified single-shooting algorithm are discussed next. Remember that these results may vary for different algorithms, but they do provide a good representation of the types of results that may be obtained. A plot showing the initial guesses for $\dot{y}_0$ versus the corresponding converged values with $\Delta\dot{y}_0 = 0.001$ is shown in Figure 5. Here, it was found that negative values of $\dot{y}_0$ generally resulted in stable orbits, so only the range containing unstable orbits is shown. It can be seen from the plot, that nearby initial guesses for $\dot{y}_0$ often converge on the same orbit with the same $\dot{y}_0$. There are significant regions where this is not the case though. For some nearby initial guesses, multiple different

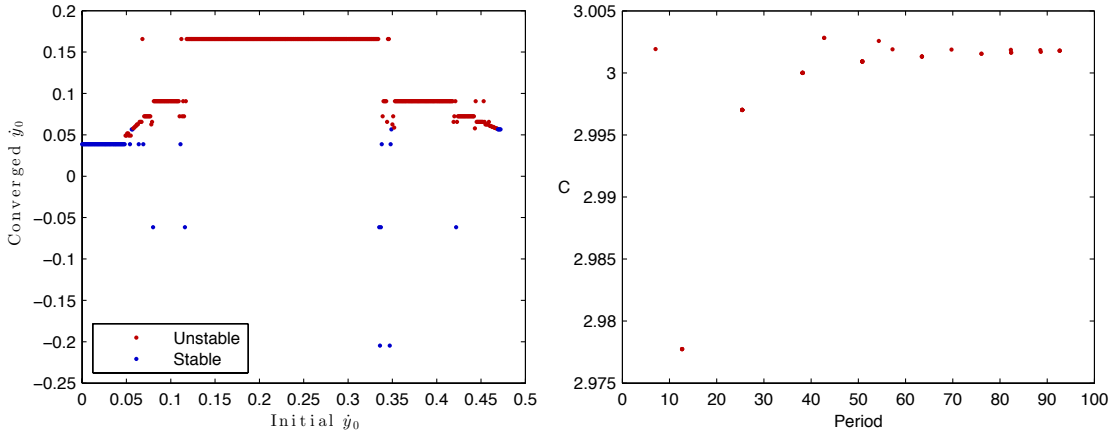

(a) Initial vs. converged $\dot{y}_0$

(b) Jacobi constant plotted versus dimensionless period for the converged unstable periodic orbits

Figure 5. Characteristics of the converged unstable periodic orbits for $x = 1.01$ and $\Delta\dot{y}_0 = 0.001$.

periodic orbits are obtained. This result may partly arise from the dynamics and partly from the particular setup of the single-shooting algorithm. What is most interesting is that in some cases the same periodic orbit will be reached for different initial $\dot{y}_0$ values with different solutions obtained in between. For example, the long line of unstable orbit cases from $\dot{y}_0 \approx 0.35$ to $\dot{y}_0 \approx 0.42$ converges on the same solution followed by several cases reaching a different orbit and then converging back to the same solution when $\dot{y}_0 = 0.45$.

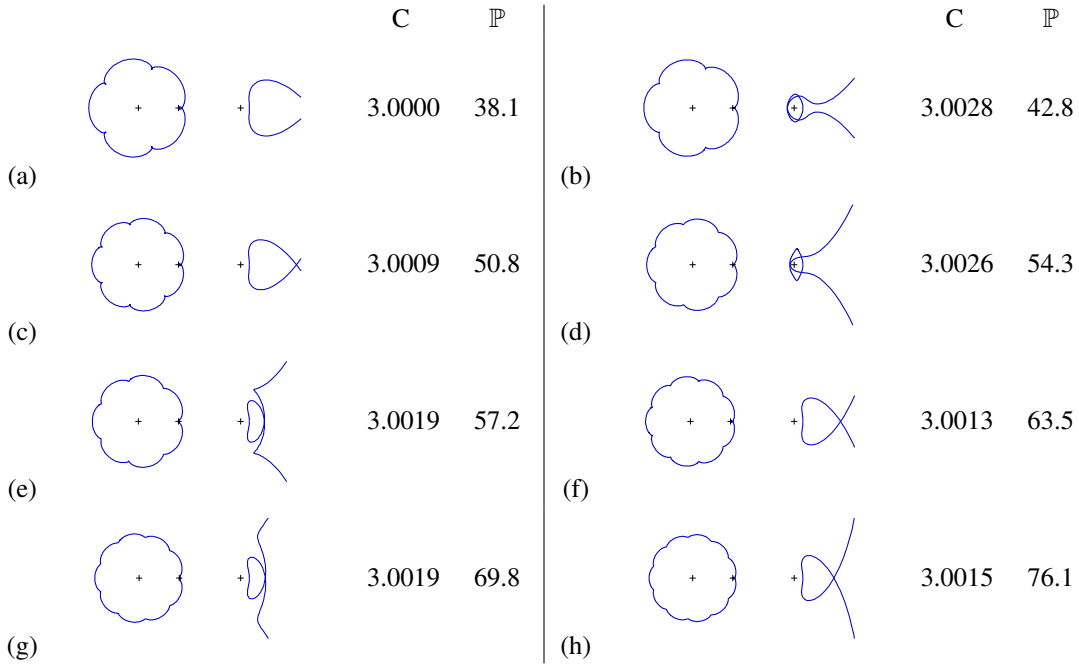

Figure 6. Periodic orbits corresponding to the points in Figure 5(b). Each orbit is plotted using the same scale with the overview orbit on the left, and a close view near the secondary on the right.

A more useful way of plotting the results is to plot the Jacobi constant versus period ($\mathbb{P}$) for each of the converged resonant orbits as seen in Figure 5(b). In this case, only the unstable periodic orbits that were obtained are plotted, and it can be seen that 16 periodic orbits were found over this interval using this method. While some of the solutions merely reproduce those orbits that are found using other methods, several solutions possess unique characteristics near the secondary. A sample of the types of orbits that were computed as a result of this narrow search is given in Figure 6. Since we are primarily concerned with comparing the topological characteristics of the solutions, the axes for these plots are omitted. However, the scales are the same for each orbit to allow a more direct comparison. Examining orbits a, c, f, and h reveals that they appear to be similar to orbits that could be found using continuation from two-body initial guesses. The number of periapses can be counted to aid in determining the resonance, and the period itself can be used to estimate the number of revolutions of the secondary. The ratio of the period of orbit a to the secondary is approximately 6.064 indicating that the orbit completes five revolutions for every six of the secondary. If the two-body osculating period is taken at $y = 0$, $x < 0$, it is found to be approximately 1.201, also confirming that the orbit is near the 5:6 resonance. A similar calculation indicates that orbit c is near the 7:8 resonance, but one difficulty with this method for computing resonance is encountered when comparing to orbit e. Orbit e appears to generally follow a Lypanov orbit near the secondary before leaving the system and consequently spends more time in this region making the overall period of the orbit larger. The normalized two body period computed at $y = 0$, $x < 0$ is still very near the period of a 7:8 resonant orbit (≈ 1.141), but the secondary has now completed approximately 9.1 revolutions in this time period. And although approximately seven periapses are seen for the orbit in the overall plot, it is not clear how to count the periapses near the secondary. So in these cases it is often useful to account for both the osculating two-body period of the orbit and the CRTBP period in order to convey an accurate description of the orbit.

Finally, it is interesting to examine the b and d orbits. In both these cases, the orbits complete revolutions around the secondary, which is potentially very desirable, and it appears that these types of orbits exist here for two different resonances. Although they appear to be similar to the corresponding orbits a and c, respectively, they both have significantly higher overall periods as a result of their loitering time near the secondary. They are also both found here for higher C values (lower energies), although it is likely possible to continue them to lower C values.

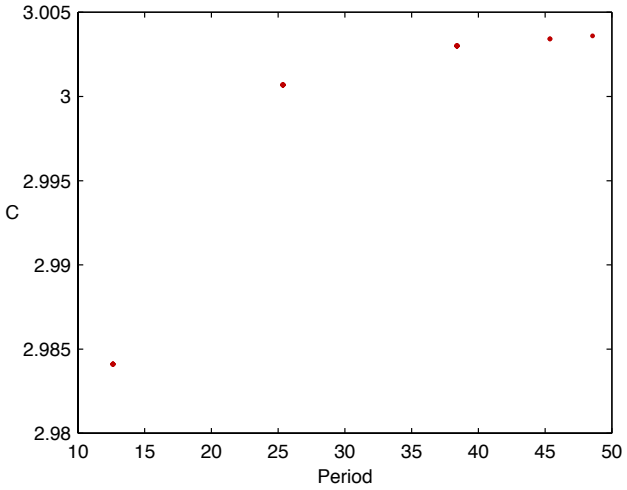

Figure 7. Characteristics of the converged unstable periodic orbits for $x = 1.02$, $\Delta\dot{y}_0 = 0.001$, and $0.0 \leq \dot{y}_0^i \leq 0.5$.

A variety of different orbits have been found for this particular x_0, and one question to answer is how do the converged orbits vary as the grid search is adjusted in x_0? If the grid search is moved further from the secondary to $x = 1.02$ using the same range of $\dot{y}_0$, the variety of orbits with loops near the secondary decreases, and the majority of the orbits found over this range are the type that would typically be found by

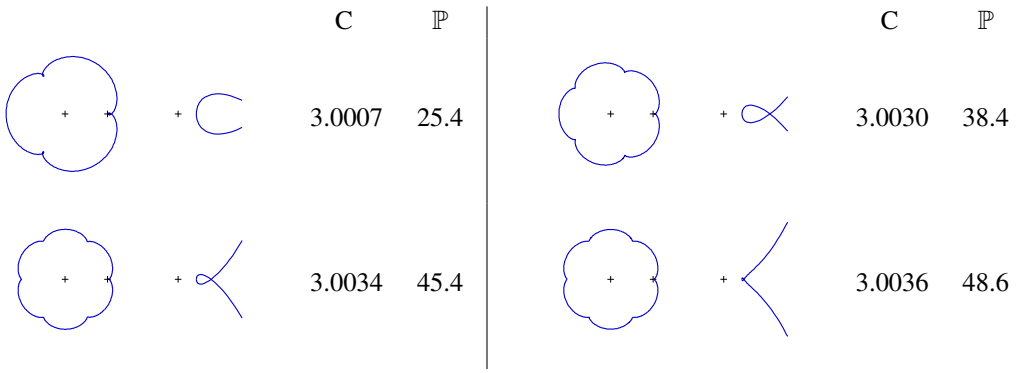

Figure 8. Periodic orbits corresponding to the points in Figure 7. Each orbit is plotted using the same scale with the overview orbit on the left, and a close view near the secondary on the right.

continuation from a two-body initial guess. This result does make sense because the effect of the secondary is decreasing as the orbit moves away from the secondary. Note that some additional orbit types may be found by decreasing the step size of $\dot{y}_0$, but these results show the effect of moving in x_0 using a direct comparison. The converged orbits for this case are plotted for each $\mathbb{P}$ and C in Figure 7, and a sample of the resulting orbits are shown in Figure 8. For these cases, the typical 3:4 and 5:6 resonant orbits are recovered, but the unusual orbits with additional loops are not found using this x_0 and $\Delta\dot{y}_0$.

More interesting results are obtained if x_0 is moved closer to the secondary. The results for this case with $x_0 = 1.005$ are plotted in Figure 9. It is immediately obvious from the plot that more solutions were captured by the search algorithm. If some of the orbits corresponding to the points in the plot are examined

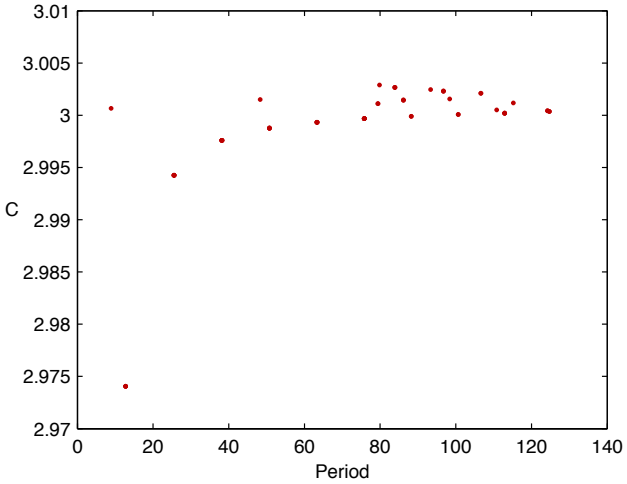

Figure 9. Characteristics of the converged unstable periodic orbits for $x = 1.005$ and $\Delta\dot{y}_0 = 0.001$, and $0.0 \leq \dot{y}_0^i \leq 0.5$.

in configuration space as shown in Figure 10, it can be seen that a wider variety of orbits are obtained. In this case, representative orbits of each type are given although more orbits with similar characteristics may exist at other resonances. The same types of 3:4 and 5:6 resonant orbits found earlier are still found with this technique. However, some orbits now appear to pass through $x = 1.005$ and move into the interior region for the majority of their orbit around the barycenter. A number of orbits with larger TOFs are found, and some unexpected orbits such as the one at (3.0025, 93.3) are captured as a result of the algorithm's reliance on the number of perpendicular crossings of the orbit. The orbit at (3.0015, 48.3) shows similar characteristics to

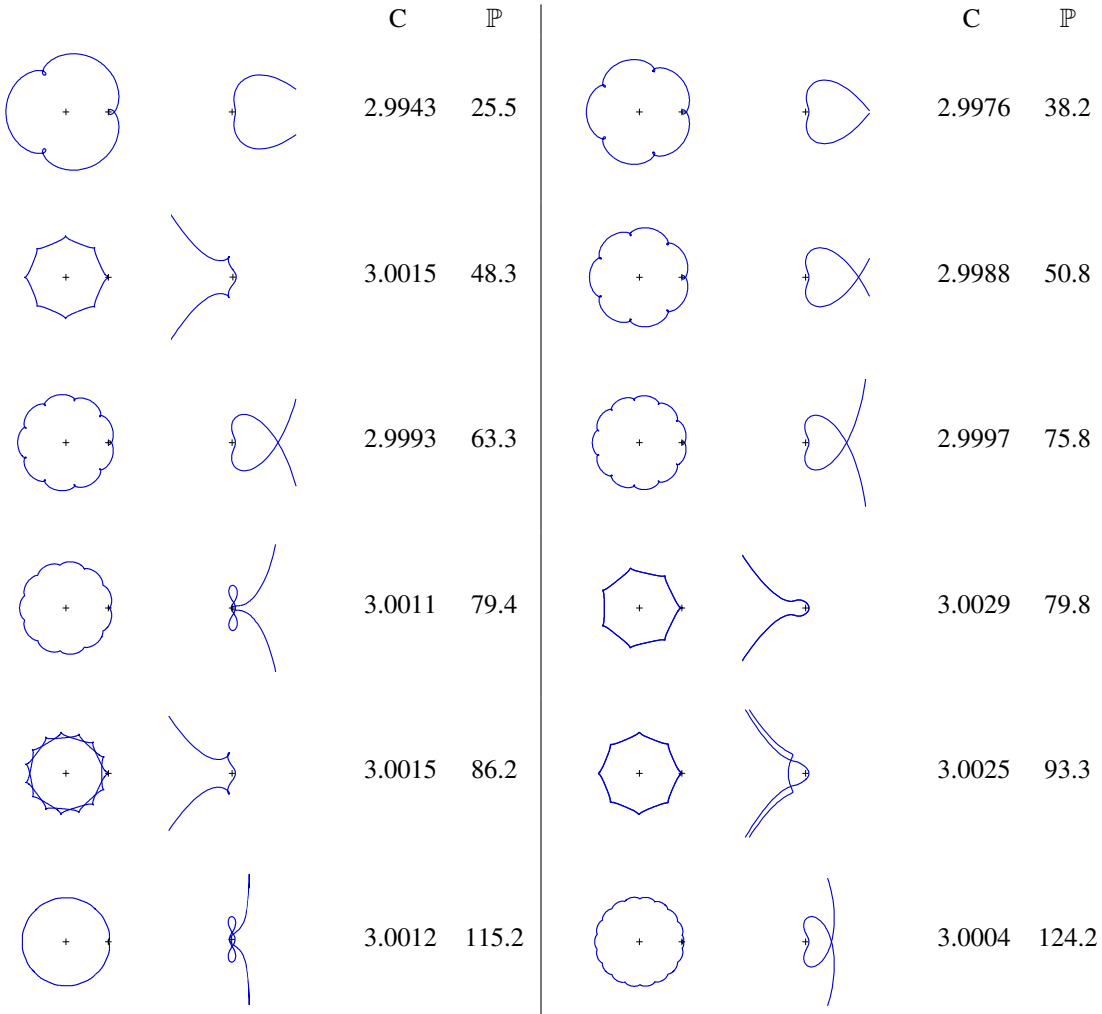

Figure 10. Periodic orbits corresponding to the points in Figure 9. Each orbit is plotted using the same scale with the overview orbit on the left, and a close view near the secondary on the right.

those orbits found near the 5:6 resonance passing on the other side of Europa. A new type of orbit is also found here with multiple loops such as for the case at (3.0011, 79.4). Orbits of this type will also be found using the techniques in the next section.

Remember only a small sample of the results from this grid search have been shown here given space constraints. Additional combinations of $(x_0, \dot{y}_0)$ have also been searched, and variations in μ and number of intersections result in a wide variety of orbits. This grid search method does require the specification of the number of intersections, and when the number of intersections becomes large, the algorithm has increasing difficulty converging. It is therefore convenient to investigate other methods that allow for searches that may more easily find trajectories with multiple intersections and trajectories with multiple loops near the secondary.

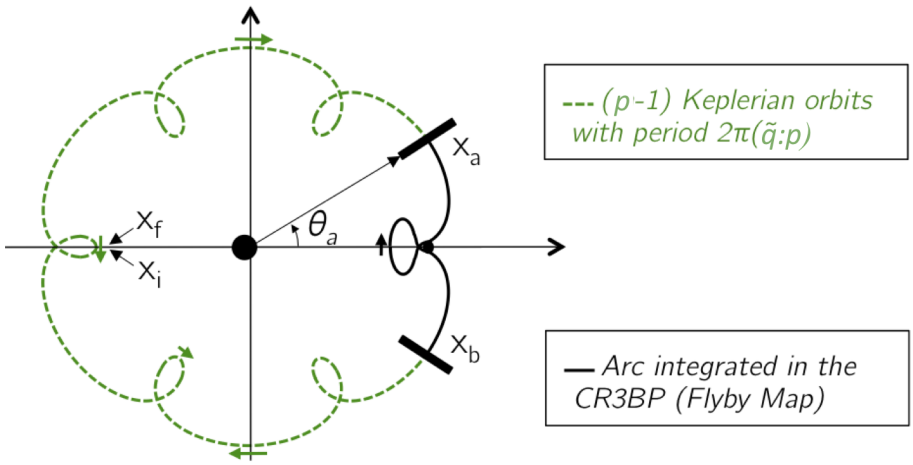

Figure 11. Resonant periodic orbit in the CWIC model

PERIODIC ORBITS IN THE CWIC MODEL

Families of periodic orbits in the PCRTBP are represented by one-dimensional curves on a 3-dimensional Poincaré section. Starting from one periodic orbit, other orbits in the same family can be computed using continuation methods. If a bifurcation point is found, the connected branches can be computed as well.

Yet finding disconnected branches or computing a global graph of the main branches is only possible by sampling a wide range of initial conditions on a fine grid. In this section, periodic orbits are computed in the simplified model CWIC ("Conics, when I can"), which approximates the CRTBP well but is less computationally demanding. Millions of candidate trajectories are computed in less than a hour on a laptop machine (1.6 GHz Intel Core i5, 4GB RAM). Specific trajectories are used in the next sections as first-guess solutions for the computation of periodic orbits in the CRTBP. Given the scope of the problem, this section focuses on the particular case of the 4:5 resonance in the Jupiter-Europa system.

CWIC

CWIC is a simplified model to describe the motion of the massless point around a major body, with the gravitational perturbation of one or more minor bodies. The perturbations are included only when the spacecraft enters a given neighborhood of the perturbing body.

In this section, we compute resonant periodic orbits in the CWIC model; trajectories are divided by Poincaré sections at apocenter (if $p : q < 1$) or pericenter (if $p : q > 1$), and Keplerian motion is assumed for each arc, except for those where the spacecraft approaches the minor body. In this last case, Eq. (1) are integrated numerically. More details on the CWIC model are found in Campagnola, Skerritt, and Russell.[48]

Figure 11 shows a schematic $p : q$ resonant periodic orbit in the CWIC model, with $p = 6$ and $q = 7$. The numerical integration is only performed between the apocenter states x_a and x_b (solid line). The Keplerian part of the orbit (dashed line) consists of $p - 1$ revolutions in the inertial frame with Tisserand constant

$$T = \frac{1}{a} + \sqrt{a(1-e^2)} \approx C \tag{10}$$

and Keplerian period $2\pi\,(\tilde{q}/p)$, where $\tilde{q}$ is a real number close to q.

Figure 11 also shows the point x_i, which is the state of the spacecraft $(p-1)/2$ revolutions before x_a; and the point x_f, which is the state of the spacecraft $(p-1)/2$ revolutions after x_b. By definition, x_i and x_f are also apsidal points, and since the orbit is symmetric and periodic, x_i coincide with x_f. Also, $\theta_f = \theta_i = -\pi$.

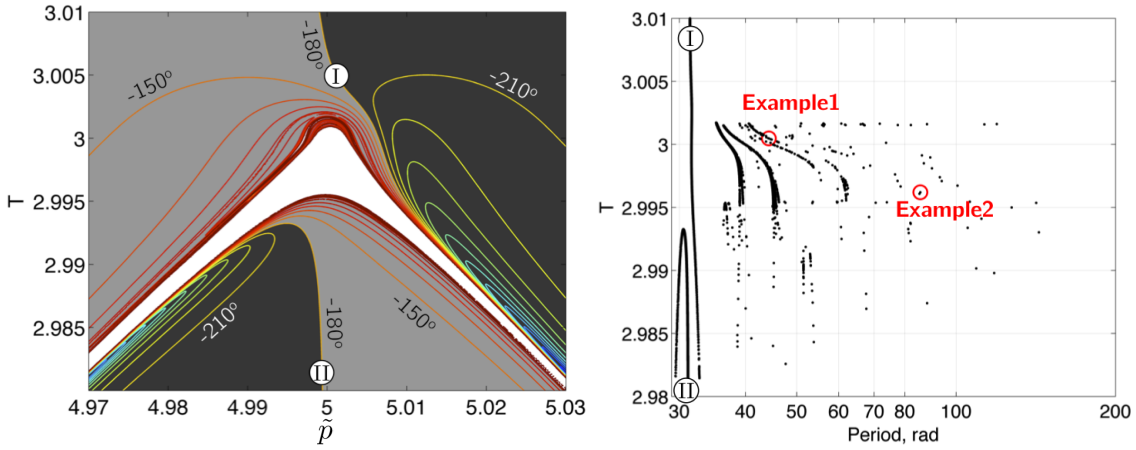

(a) Level-sets of θ_f

(b) Elements of $\mathcal{S}_\epsilon$ revealing different families of periodic orbits

Figure 12. Grid search of $p:q$ periodic orbits at Europa.

Note that the conditions $\theta_f = \theta_i = -\pi$ alone guarantee the existence of two perpendicular crossings of the negative x-axis, and hence the existence of a periodic orbit.

Grid Search

For a given p, and assuming $\theta_i = -\pi$, the final angular position θ_f is a function of the initial conditions $(T_i, \tilde{q}_i)$, and resonant periodic orbits are elements of the set $\mathcal{S} = \theta_f^{-1}(-\pi)$. In practice, it may be easier to find quasi-periodic orbits defined by the set $\mathcal{S}_\epsilon = \{(\tilde{q}_i, T_i) : |\theta_f(\tilde{q}_i, T_i) + \pi| < \epsilon\}$ for some small positive ϵ (note that $\lim_{\epsilon \to 0} \mathcal{S}_\epsilon = \mathcal{S}$).

Elements of $\mathcal{S}_\epsilon$ are computed with a grid-search algorithm; initial conditions $(T_i, \tilde{q}_i)$ on a two-dimensional grid are mapped to the final condition θ_f, and candidate periodic orbits are stored. The mapping occurs in three steps (see Fig.11): (1) starting from $T_i, \tilde{q}_i$, and p, the coordinates (a_a, T_a, λ_a) of the point x_a are calculated using

$$T_a = T_i, \; a_a = \sqrt[3]{\frac{(\tilde{q}/p)^2}{1-\mu}}, \; \lambda_a = \pi - (\tilde{q}\pi \mod 2\pi), \tag{11}$$

where λ_a is the argument of the apsis of reference (see Campagnola et al.[48]); (2) the coordinates (a_a, T_a, λ_a) of x_a are mapped to the coordinates (a_b, T_b, λ_b) of x_b using the Flyby Map (see Campagnola et al.[48]); (3) the final angular position is computed using

$$\theta_f = \lambda_b - \left(2\pi \sqrt{\frac{a_b^3}{1-\mu}} \mod 2\pi \right) \frac{p}{2}. \tag{12}$$

Figure 12(a) shows the level-sets of the function $\theta_f(\tilde{q}_i, T_i)$ (in degrees) in the Europa-Jupiter system for $p = 4$, $q = 5$. The dark gray domain corresponds to $\theta_f < -180^o$. The light gray domain corresponds to $\theta_f > -180^o$. The white area corresponds to trajectories that are filtered out because they enter the inner region with $\tilde{q}_f/p < 1$. The curves labeled I and II are subsets of $\mathcal{S} = \theta_f^{-1}(-180^o)$ and represent resonant periodic orbits with type I and type II flybys.[48] Other subsets of S are deep in the chaotic region between the white and grey areas and cannot be easily seen in this graph.

Elements of $\mathcal{S}_\epsilon$ (with $\epsilon = 1$ deg) are shown on Figure 12(b), where the x-axis represents the actual period (in the rotating frame). Periodic orbits with type I and type II flybys appear at low periods, while at higher

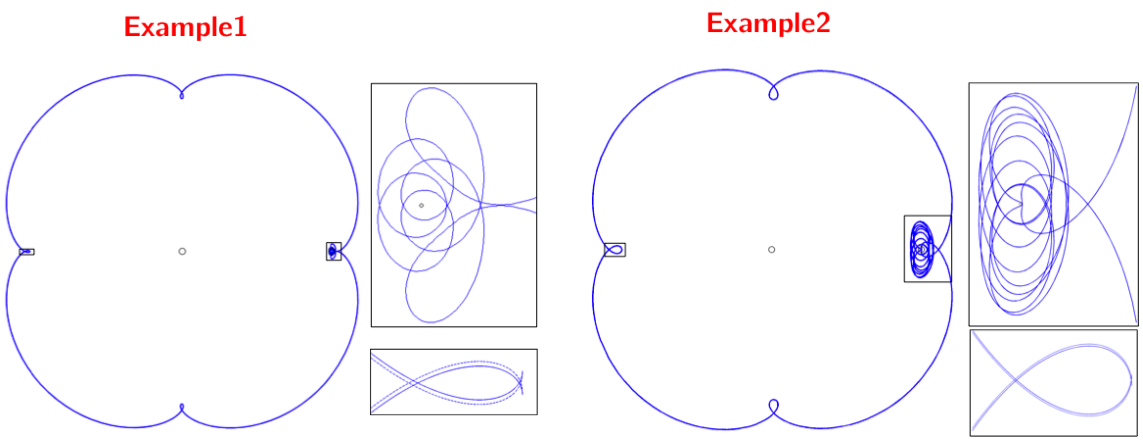

Figure 13. Quasi-periodic orbits in the CWIC model (dashed lines) and in the CRTBP model (solid lines).

periods clusters of points reveal families of solutions that differ by the number of revolutions around the secondary. Two example solutions are shown in Figure 13, where the dashed line is the orbit in the CWIC model, and the solid line is the orbit fully integrated in the PCRTBP. Neither trajectory is exactly periodic ($x_i \neq x_f$), because of the tolerance ϵ allowed on the final θ_f. The figure shows that the approximation introduced by the CWIC model results in a small error. If the error is small enough, the trajectory may be used as an initial guess for a differential corrector.

CONVERGED PERIODIC ORBITS FROM THE CWIC METHOD

One of the advantages of the CWIC model is that it allows many different trajectories to be computed and evaluated rapidly. Once the periodic orbits are computed they can be plotted individually to find orbits with potentially desirable characteristics. Once such an orbit is found, the initial guess may be used in a differential corrector to verify that a truly periodic orbit exists with these characteristics. This process was completed for several different selected points from the plot in Figure 12(b). The resulting orbits are shown in Figure 14, and their location in the plot is designated by $\mathbb{P}$ and $C \approx T$. In each case the converged orbits possessed very

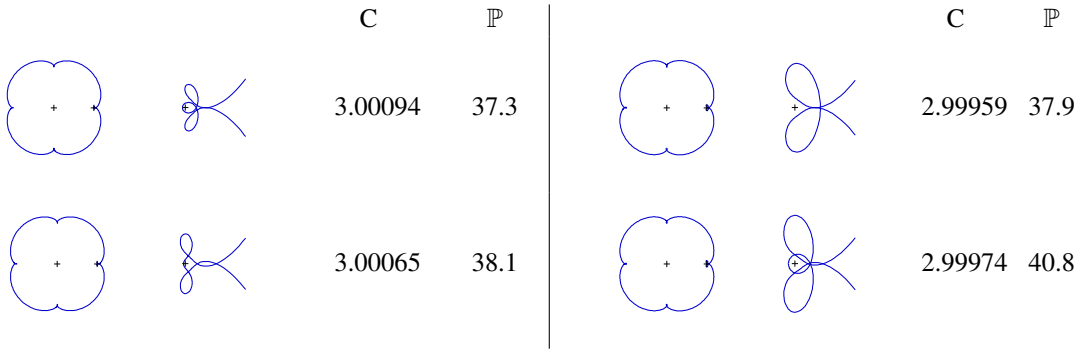

Figure 14. Converged cases from the CWIC method.

similar characteristics to the orbits found using the CWIC method, and the final values of C and $\mathbb{P}$ matched the predicted values closely. In these cases, the CWIC method generally allows the computation of trajectories with multiple loops near the secondary that are difficult to find using the single-shooting grid search discussed earlier. These types of orbits have potential applications for mission design since they allow a spacecraft to approach the secondary for observations multiple times at different orientations. It is worth noting that for

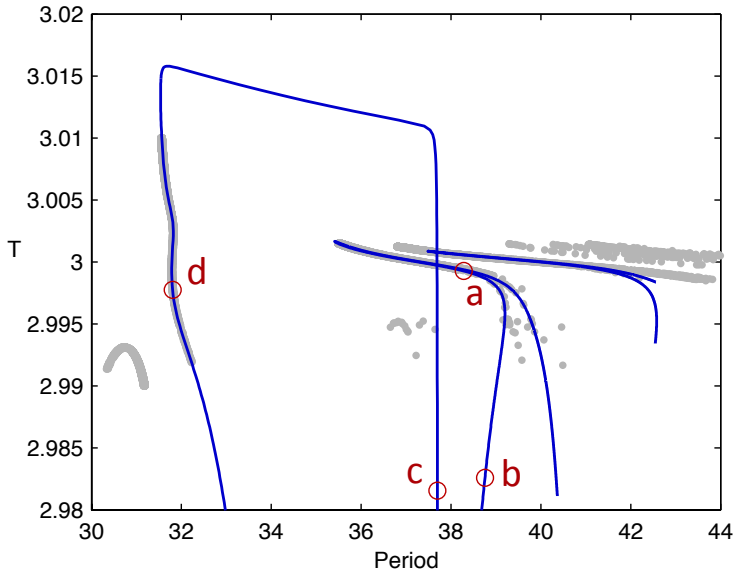

Figure 15. Comparison of families computed by continuation to the predictions using the CWIC method. The continuation results are in blue with the output from the CWIC method plotted as points in gray. Several specific orbits selected for further analysis are labeled with red circles. Note that the red points all fall on a line resulting from the same orbit continuation, while the blue line in the upper right is the result of the continuation of a different orbit.

these particular cases, even though the resonance used for the search was a 4:5 resonance, the period of the orbits themselves can vary significantly. As expected, this result is primarily a function of the number of loops the trajectory has near the secondary and the amount of time it spends there. The osculating two-body period far from the secondary remains near the 4:5 resonance, and except for the multiple loops near the secondary, the trajectory has the typical four major periapses common to the 4:5 resonant orbits. Note that the solutions at C = 3.00094 and C = 2.99974 are the same topologically, but their actual periods vary significantly. This result highlights the fact that orbits within the same family may have noticeably different periods depending on the Jacobi constant. Once the converged solutions have been obtained it is possible to continue them to determine how closely the families match the predictions from the CWIC method.

CONTINUATION OF ORBIT SOLUTIONS

Once particular orbit solutions have been found using one of the search algorithms, the resulting orbit may be continued using a variety of techniques. Simpler techniques may be used to extend the families over short intervals, while the continuation techniques implemented in AUTO[49] are well suited to broader explorations of the orbit families. In this section, simpler continuation techniques are initially used to extend the families, and the pseudo-arclength continuation methods in AUTO are used to deal with fold points. Because a full exploration of each orbit would take more space than is available here, several representative cases are examined in detail next.

Continuation of Orbit Solutions from CWIC

The converged solutions were used to search for families of orbits using continuation with linear extrapolation and with the pseudo-arclength continuation methods of AUTO. A comparison of the orbits computed using these methods and the results from the CWIC method is given in Figure 15 for a subset of the orbits. It can be seen from the plot that the CWIC results match the continuation plots for those families chosen for the continuation. A number of families and orbits still remain for further analysis, but these results indicate that the CWIC results will serve as a good predictor of resonant orbits.

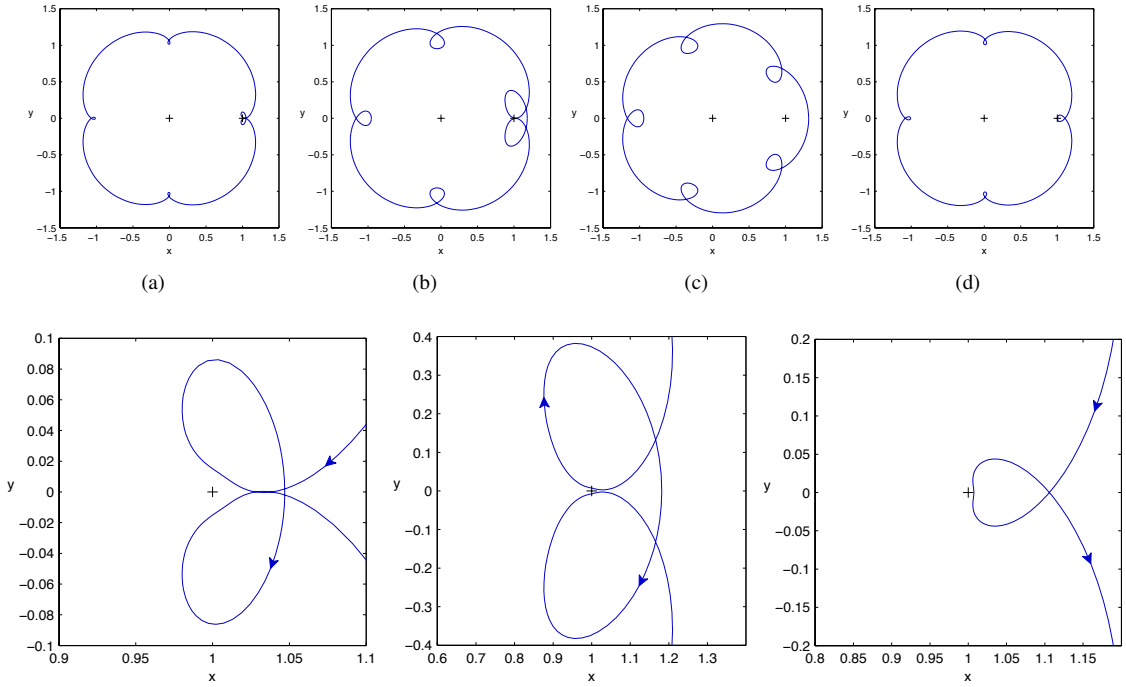

(a) (b) (c) (d)

(e) Closer view of case a near secondary (f) Closer view of case b near secondary (g) Closer view of case d near secondary

Figure 16. Selected orbits from the continuation plots in Figure 15. The labeled points circled in that figure correspond to the orbits shown here.

A selection of the orbits from the continuation process are plotted in configuration space in Figure 16. The changes in the orbits over the continuation process can be observed from these plots, and it is apparent that some of the different types of orbits that have been obtained using various grid searches may in fact be related. Cases a and b possess similar characteristics although case a has smaller loops near the secondary (note the change in scale in the close views). The continuation continues until orbits of the type found in case d are found. These orbits were also predicted from the CWIC method, and they are of the same type that may typically be found using continuation from two-body initial conditions. Another interesting result though is that the continuation proceeds through the stable orbit found in case c. The CWIC method was set up to search for unstable orbits, so these types of orbits were not found in this search. The fact that the continuation proceeded through a stable resonant orbit is interesting, and deserves further analysis. A more in-depth analysis of this type of case is undertaken in the next section.

Continuation of a 3:4 Resonant Orbit Solution

This analysis focuses on the details of the continuation of a typical 3:4 resonant orbit computed in the Jupiter-Europa system. The orbits computed through the continuation process are represented as dots plotted as the Jacobi constant versus $\mathbb{P}$ in Figure 17(a). The orbits resulting from the continuation are plotted in configuration space in Figure 17(b). In each case the stable orbits are plotted as blue, and the unstable orbits are plotted as red. It can be seen from the plots that those orbits that are unstable correspond to the orbits with a periapse near Europa. As the orbits evolve to stable orbits, the periapses move to either side of Europa, and the apoapse of the orbit occurs near Europa.

Examining the continuation plot in Figure 17(a) reveals that two different type of orbits in the continuation exist for the same value of the Jacobi constant over a selected range. It is interesting to compare these different orbits using a Poincaré section,[11] and such a comparison is made for C = 3.0 with a surface of section defined by $y = 0, x < 0$ in Figure 18. It can be easily seen that, as would be expected, the unstable resonant

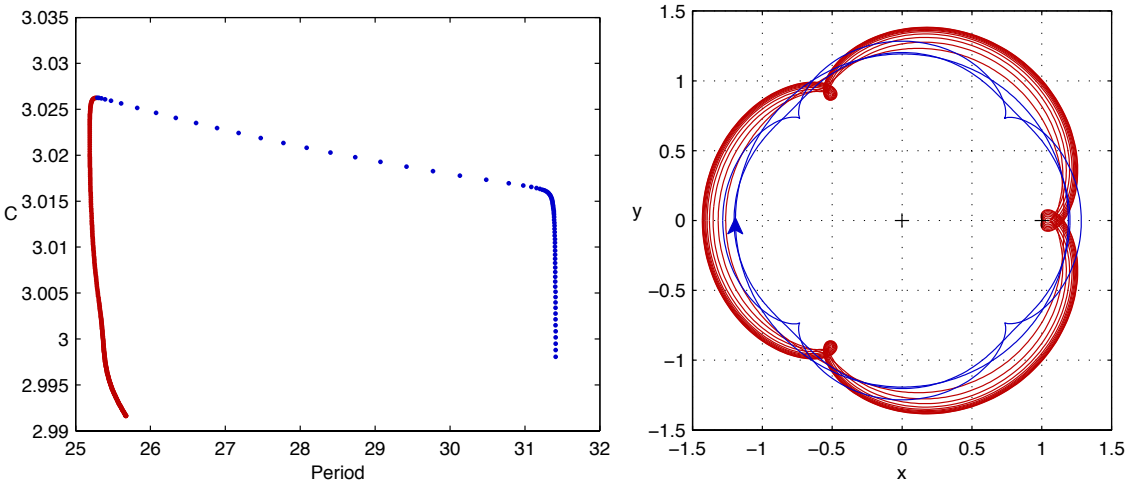

(a) Continuation plot of trajectories

(b) Trajectories plotted in the plane

Figure 17. Sample of results from the continuation of a 3:4 resonant orbit in the Jupiter-Europa system. A subset of the trajectories in the continuation plot are given in the plot in the xy plane. Unstable resonant orbits are plotted in red while stable resonant orbits are plotted in blue.

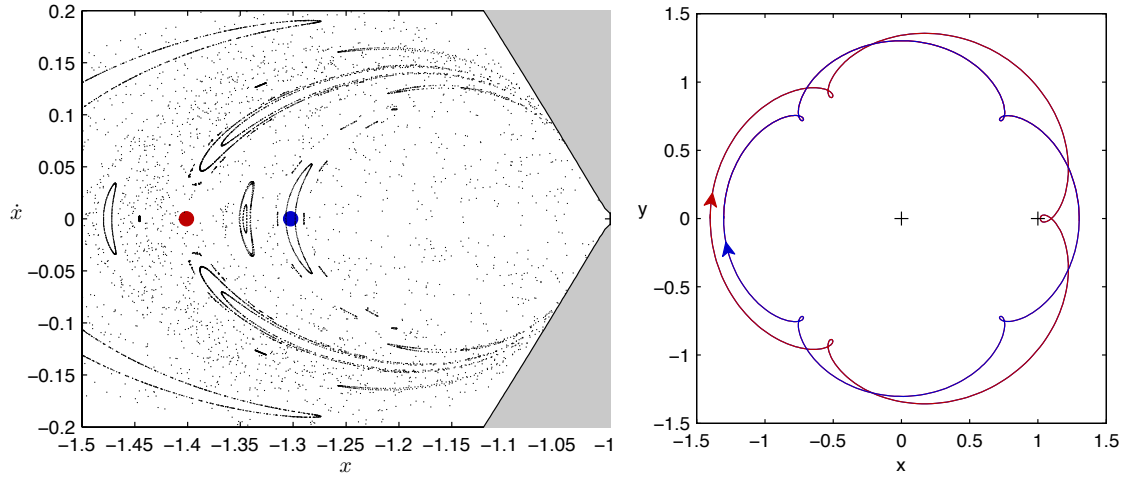

(a) Poincaré section comparing trajectory intersections

(b) Orbits corresponding to those in the Poincaré section

Figure 18. Poincaré section and corresponding orbits in configuration space for C = 3.0 with a surface of section defined by $y = 0, x < 0$.

orbit lies in the chaotic sea while the stable resonant orbit is at the center of one of the stable islands. The periods of the orbits at the Poincaré section indicate that the unstable and stable orbits are near the 3:4 and 4:5 resonances, respectively. If the Poincaré sections are generated closer to the transition between the two orbits the two orbits can be seen to approach one another as expected in Figure 19(a). The unstable resonant orbit comes closer to the stable quasi-periodic orbit at this energy as the two orbits approach one another in the continuation. The orbits in the plane approach one another and both approach a more circular orbit as shown in Figure 19(b). These results suggest that finding unstable resonant orbits by continuation of stable resonant orbits may be a feasible method for finding these orbits. With the use of the pseudo-arclength techniques this

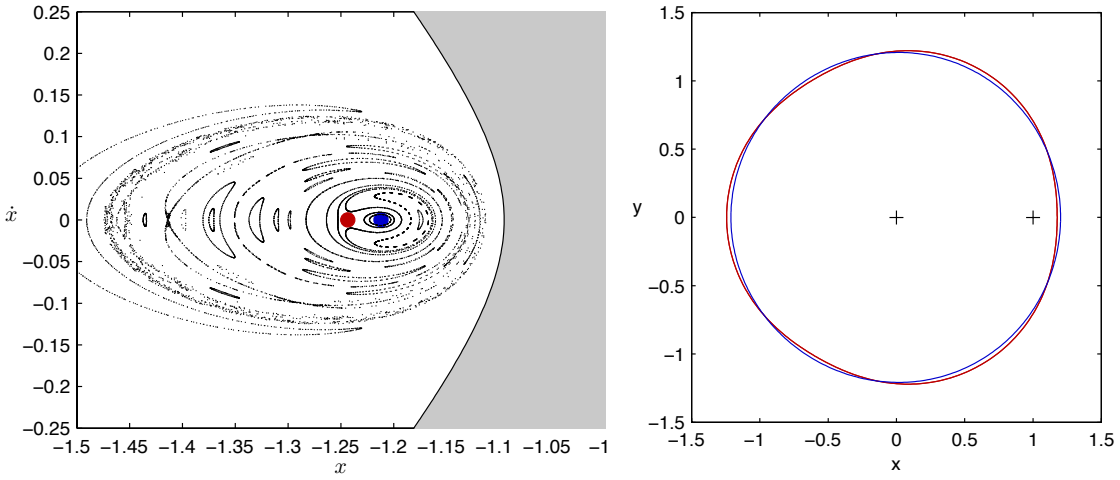

(a) Poincaré section comparing trajectory intersections

(b) Orbits corresponding to those in the Poincaré section

Figure 19. Poincaré section and corresponding orbits in configuration space for C = 3.0258 with a surface of section defined by $y = 0, x < 0$.

process does seem to be possible for specific cases. This process has been completed for the given example by starting with the converged stable solution and continuing to the unstable resonant orbits.

CONCLUDING REMARKS

Several different techniques for computing unstable resonant orbits have been explored, and a sample of the large range of possible results have been presented for specific cases. The single-shooting grid search method successfully produced unique orbits across a wide range of resonances that can be used as seeds to compute new families. It was found that it is ideally suited for trajectories with fewer intersections because of numerical limitations. The flyby map technique addressed this issue and was shown to successfully compute families of trajectories at the 4:5 resonance with multiple intersections. The results were found to serve as useful initial guesses for convergence to truly periodic resonant orbits. Continuation of specific trajectories were also shown to closely match the results from the flyby map technique. Finally, it was shown to be feasible to use the continuation process to compute unstable resonant orbits from stable resonant orbits for particular cases.

FUTURE WORK

Future work will include the exploration of additional systems and families with both the single-shooting method and the flyby map method. The feasibility of computing unstable resonant orbits using different continuation methods will also be further explored. Additional results from other systems and resonances will also be documented as part of our broader study.

ACKNOWLEDGEMENTS

The research presented here has been carried out at the Jet Propulsion Laboratory, California Institute of Technology, under a contract with the National Aeronautics and Space Administration. Funding for this research came from AMMOS/MGSS under the “Tour and Endgame Design using Invariant Manifolds” study. The authors would like to thank Martin Lo, Jon Sims, Try Lam, and Channing Chow for their helpful comments and conversations.

REFERENCES

[1] J. A. Sims and J. M. Longuski, "Analysis of V_∞ Leveraging for Interplanetary Missions," *AIAA/AAS Astrodynamics Conference*, No. AIAA-1994-3769, Scottsdale, Arizona, August 1-3 1994.

[2] S. Campagnola and R. Russell, "Endgame Problem Part 1: V-Infinity-Leveraging Technique and the Leveraging Graph," *Journal of Guidance, Control, and Dynamics*, Vol. 33, No. 2, 2010, pp. 463–475.

[3] R. C. Woolley and D. J. Scheeres, "Hyperbolic Periodic Orbits in the Three-Body Problem and their Application to Orbital Capture," *AAS George H. Born Symposium*, Boulder, Colorado, May 13-14 2010.

[4] S. Campagnola and R. Russell, "Endgame Problem Part 2: Multibody Technique and the Tisserand-Poincare Graph," *Journal of Guidance, Control, and Dynamics*, Vol. 33, No. 2, 2010, pp. 476–486.

[5] S. D. Ross and D. J. Scheeres, "Multiple Gravity Assists, Capture, and Escape in the Restricted Three-Body Problem," *Siam Journal On Applied Dynamical Systems*, Vol. 6, 2007, pp. 576–596.

[6] G. J. Whiffen, "Mystic: Implementation of the Static Dynamic Optimal Control Algorithm for High Fidelity Low Thrust Trajectory Design," *AIAA/AAS Astrodynamics Specialists Conference*, No. AIAA-2006-6741, Keystone, Colorado, August 21-24 2006.

[7] G. J. Whiffen and T. Lam, "The Jupiter Icy Moons Orbiter Reference Trajectory," *AAS/AIAA Space-Flight Mechanics Meeting*, No. AAS 06-186, Tampa, Florida, January 22-26 2006.

[8] C. G. Schroer and E. Ott, "Targeting in Hamiltonian Systems that have Mixed Regular/Chaotic Phase Spaces," *Chaos*, Vol. 7, December 1997, pp. 512–519.

[9] E. Bollt and J. D. Meiss, "Targeting Chaotic Orbits to the Moon through Recurrence," *Physics Letters A*, Vol. 204, August 28 1995, pp. 373–378.

[10] R. L. Anderson and M. W. Lo, "A Dynamical Systems Analysis of Planetary Flybys and Approach: Ballistic Case," *The Journal of the Astronautical Sciences*, Vol. 58, April-June 2011, pp. 167–194.

[11] R. L. Anderson and M. W. Lo, "Dynamical Systems Analysis of Planetary Flybys and Approach: Planar Europa Orbiter," *Journal of Guidance, Control, and Dynamics*, Vol. 33, November-December 2010, pp. 1899–1912.

[12] R. L. Anderson and M. W. Lo, "Role of Invariant Manifolds in Low-Thrust Trajectory Design," *Journal of Guidance, Control, and Dynamics*, Vol. 32, November-December 2009, pp. 1921–1930.

[13] G. Lantoine, R. P. Russell, and S. Campagnola, "Optimization of Low-Energy Resonant Hopping Transfers between Planetary Moons," *Acta Astronautica*, Vol. 68, April-May 2011, pp. 1361–1378.

[14] R. L. Anderson and M. W. Lo, "Flyby Design using Heteroclinic and Homoclinic Connections of Unstable Resonant Orbits," *21st AAS/AIAA Space Flight Mechanics Meeting*, No. AAS 11-125, New Orleans, Louisiana, February 13-17 2011.

[15] R. L. Anderson, "Tour Design Using Resonant Orbit Heteroclinic Connections in Patched Circular Restricted Three-Body Problems," *23rd AAS/AIAA Space Flight Mechanics Meeting*, No. AAS 13-493, Kauai, Hawaii, February 10-14 2013.

[16] R. L. Anderson, "Approaching Moons from Resonance via Invariant Manifolds," *22nd AAS/AIAA Space Flight Mechanics Meeting*, No. AAS 12-136, Charleston, South Carolina, January 29 - February 2 2012.

[17] R. L. Anderson and M. W. Lo, "Spatial Approaches to Moons from Resonance Relative to Invariant Manifolds," *63rd International Astronautical Congress*, No. IAC-12.C1.7.4, Naples, Italy, International Astronautical Federation, October 1-5 2012.

[18] M. W. Lo and J. S. Parker, "Unstable Resonant Orbits near Earth and Their Applications in Planetary Missions," *AIAA/AAS Astrodynamics Specialist Conference*, Providence, Rhode Island, August 16-19 2004, pp. Paper AIAA 2004–22819.

[19] M. Vaquero and K. C. Howell, "Design of Transfer Trajectories Between Resonant Orbits in the Restricted Three-Body Problem with Application to the Earth-Moon System," *1st IAA/AAS Conference on the Dynamics and Control of Space Systems*, Porto, Portugal, March 19-21 2012.

[20] M. Vaquero and K. Howell, "Leveraging Resonant Orbit Manifolds to Design Transfers Between Libration Point Orbits in Multi-Body Regimes," *23rd AAS/AIAA Space Flight Mechanics Meeting*, No. AAS 13-334, Kauai, Hawaii, February 10-14 2013.

[21] E. Barrabés and G. Gómez, "Spatial p-q Resonant Orbits of the RTBP," *Celestial Mechanics and Dynamical Astronomy*, Vol. 84, 2002, pp. 387–407.

[22] E. Barrabés and G. Gómez, "Three-Dimensional p-q Resonant Orbits Close to Second Species Solution," *Celestial Mechanics and Dynamical Astronomy*, Vol. 85, 2003, pp. 145–174.

[23] E. Barrabés and G. Gómez, "A Note on Second Species Solutions Generated From p-q Resonant Orbits," *Celestial Mechanics and Dynamical Astronomy*, Vol. 88, September 2004, pp. 229–244.

[24] M. Vaquero and K. C. Howell, "Poincaré Maps and Resonant Orbits in the Circular Restricted Three-Body Problem," *AAS/AIAA Astrodynamics Specialist Conference*, No. AAS 11-428, Girdwood, Alaska, July 31 - August 4 2011.

[25] M. Hénon, *Generating Families in the Restricted Three-Body Problem*, Vol. 52 of *Lecture Notes in Physics*. New York: Springer, 1997.
[26] M. Hénon, *Generating Families in the Restricted Three-Body Problem II. Quantitative Study of Bifurcations*, Vol. 65 of *Lecture Notes in Physics*. New York: Springer, 2001.
[27] R. A. Broucke, "Periodic Orbits in the Restricted Three-Body Problem With Earth-Moon Masses," Technical Report 32-1168, Jet Propulsion Laboratory, February 15 1968.
[28] R. A. Broucke, "Periodic Orbits in the Elliptic Restricted Three-Body Problem," Tech. Rep. 32-1360, Jet Propulsion Laboratory, July 15 1969.
[29] E. Strömgren, "Connaisance actuelle des orbites dans le problème des trois corps," *Bulletin Astronomique*, Vol. 9, 1933, pp. 87–130.
[30] V. Szebehely, *Theory of Orbits: The Restricted Problem of Three Bodies*. New York: Academic Press, 1967.
[31] R. P. Russell, "Global Search for Planar and Three-Dimensional Periodic Orbits near Europa," *AAS/AIAA Astrodynamics Specialist Conference*, No. Paper AAS 2005-290, Lake Tahoe, CA, August 7-11 2005.
[32] A. E. Roy and M. W. Ovenden, "On the Occurrence of Commensurable Mean Motions in the Solar System. The Mirror Theorem," *Monthly Notices of the Royal Astronomical Society*, Vol. 115, 1955, pp. 296–309.
[33] A. Miele, "Theorem of Image Trajectories in the Earth-Moon Space," *Astronautica Acta*, Vol. 6, No. 51, 1960, pp. 225–232.
[34] K. C. Howell and J. V. Breakwell, "Three-Dimensional, Periodic, 'Halo' Orbits," *Celestial Mechanics*, Vol. 32, January 1984, pp. 53–71.
[35] J. S. Parker and R. L. Anderson, *Low-Energy Lunar Trajectory Design*, Vol. 12 of *DESCANSO Deep Space Communications and Navigation Series*. Pasadena, California: Jet Propulsion Laboratory, July 2013.
[36] H. B. Keller, *Lectures on Numerical Methods in Bifurcation Problems*. New York: Springer-Verlag, 1986.
[37] E. J. Doedel and B. E. Oldeman, "AUTO-07P: Continuation and Bifurcation Software for Ordinary Differential Equations," tech. rep., Concordia University, Montreal, Canada, October 2009.
[38] C. D. Murray and S. F. Dermott, *Solar System Dynamics*. Cambridge, United Kingdom: Cambridge University Press, 1999, pp. 421-428.
[39] T. Parker and L. O. Chua, *Practical Numerical Algorithms for Chaotic Systems*. New York: Springer-Verlag, 1989, pp. 130-166.
[40] J. R. Johannesen and L. A. D'Amario, "Europa Orbiter Mission Trajectory Design," *Astrodynamics: Proceedings of the AAS/AIAA Astrodynamics Conference, August 16-19, 1999, Girdwood, Alaska* (K. C. Howell, F. R. Hoots, B. Kaufman, and K. T. Alfriend, eds.), Vol. 103, Part I of *Advances in the Astronautical Sciences*, San Diego, California, American Astronautical Society, Univelt Inc., 1999, pp. 895–908.
[41] R. L. Anderson, *Low Thrust Trajectory Design for Resonant Flybys and Captures Using Invariant Manifolds*. PhD thesis, University of Colorado at Boulder, http://ccar.colorado.edu/~rla/papers/andersonphd.pdf, 2005.
[42] G. Lantoine, R. P. Russell, and S. Campagnola, "Optimization of Low-Energy Resonant Hopping Transfer Between Planetary Moons," *60th International Astronautical Congress*, No. IAC-09.C1.1.1, Deajeon, Korea, October 12-16 2010.
[43] T. M. Vaquero Escribano, "Poincaré Sections and Resonant Orbits in the Restricted Three-Body Problem," Master's thesis, Purdue University, West Lafayette, Indiana, May 2010.
[44] K. C. Howell, B. Marchand, and M. W. Lo, "Temporary Satellite Capture of Short-Period Jupiter Family Comets from the Perspective of Dynamical Systems," *The Journal of the Astronautical Sciences*, Vol. 49, October-December 2001, pp. 539–557.
[45] W. S. Koon, M. W. Lo, J. E. Marsden, and S. D. Ross, "Resonance and Capture of Jupiter Comets," *Celestial Mechanics and Dynamical Astronomy*, Vol. 81, No. 1-2, 2001, pp. 27–38.
[46] C. Uphoff, P. H. Roberts, and L. D. Friedman, "Orbit Design Concepts for Jupiter Orbiter Missions," *Journal of Spacecraft and Rockets*, Vol. 13, No. 6, 1976, pp. 348–355.
[47] R. L. Anderson and M. W. Lo, "The Role of Invariant Manifolds in Low Thrust Trajectory Design (Part II)," *AIAA/AAS Astrodynamics Specialist Conference*, No. Paper AIAA 2004-5305, Providence, Rhode Island, August 16-19 2004.
[48] S. Campagnola, P. Skerritt, and R. P. Russell, "Flybys in the Planar, Circular, Restricted, Three-Body Problem," *Celestial Mechanics and Dynamical Astronomy*, Vol. 113, No. 3, 2012, pp. 343–368.
[49] D. J. Dichmann, E. J. Doedel, and R. C. Paffenroth, "The Computation of Periodic Solutions of the 3-Body Problem Using the Numerical Continuation Software AUTO," *International Conference on Libration Point Orbits and Applications*, Aiguablava, Spain, June 10-14 2002.